Modern Physical Chemistry Research (2024)
Clausius Scientific Press, Canada

DOI: 10.23977/mpcr.2024.040103
ISSN 2616-1702 Vol. 4 Num. 1

Research on the Gamma/Proton Identification Effect of HADAR Based on Multi-Layer Sensor

Liwu Liu[1,a], Shang Sun[1,b], Shaozhang Zhao[1,c], Dayu Peng[1,d], Xiaoyao Ma[1,e], Qi Gao[1,2,f,*]

[1]Department of Physics, College of Science, Tibet University, Lhasa, 850000, China
[2]The Key Laboratory of Cosmic Rays (Tibet University), Ministry of Education, Lhasa, 850000, China
[a]liulw@ihep.ac.cn, [b]sunlaoke@qq.com, [c]zhaosz@ihep.ac.cn, [d]pengdayu@outlook.com, [e]3066797421@qq.com, [f]fbc1980@163.com
[*]Corresponding author

Keywords: HADAR, Multilayer Perceptron, Gamma Rays

Abstract: This study aims to optimize the discrimination performance of gamma/proton in high altitude detection of astrological radiation (HADAR) experiments by employing the multilayer perceptron (MLP) algorithm. The HADAR experiment is used to observe the Cherenkov light produced by cosmic rays and gamma rays in the atmosphere via a composite array composed of four water lenses and surrounding scintillation detectors. And it is highly competitive in detecting the transient sources and the prompt emission of gamma-ray bursts due to its advantages such as low threshold energy (~30GeV) and wide field of view (~30 °). However, the image discrimination between background noise and signal become weak when the detected energy of HADAR is less than 100 GeV, leading to unsatisfactory gamma/proton discrimination performance of traditional Hillas parameter methods. In this study, we employ MLP as a discriminator to conduct training and classification based on input characteristic parameters (such as Hillas parameters and core information). The results of Monte Carlo simulation demonstrate that the MLP method exhibits excellent performance and accuracy gamma/proton identification. Specifically, the discrimination between signal and background noise is enhanced at detection energies between 30-100 GeV, and the highest achieved Q-factor is 2.17 (proton exclusion rate ~97.80%, gamma retention rate ~32.20%). This study provides valuable references and a solid foundation for enhancing the gamma/proton discrimination performance of HADAR.

1. Introduction

Very High Energy (VHE; $E \geq 30$ GeV) gamma rays are a signature of extreme physical phenomena in the universe, commonly observed in processes such as galactic nuclei (AGN [1]), gamma-ray bursts (GRB [2]) and so on. Thanks to the advancements of broad imaging atmospheric Cherenkov telescope technology (IACT [3]), researchers are able to study the physical processes of AGN or the morphology and spectra of GRBs by observing Cherenkov light generated from the interaction between cosmic rays and Earth's atmosphere. This provides an effective means for exploring the nature and origin of these extraordinary physical phenomena.

IACTs can only monitor individual sources and are unable to cover extensive celestial areas owing to the drawbacks of a narrow field of view (3.5-5 °) and short effective observation time (10%) [4]. To address this issue, the high altitude detection of astronomical radiation (HADAR) experiment, a ground-based experimental array with low threshold energy and large field of view, is proposed and carried out [5]. HADAR is a refracting ground-based telescope array based on atmospheric imaging Cherenkov technology that collects atmospheric Cherenkov light signals through a large aperture wide-angle water lens (lens + pure water) system to achieve the observation of VHE cosmic rays and gamma-rays.

However, during observation, Cherenkov photons caused by VHE gamma-rays are significantly lower compared to cosmic rays [6]. Therefore, in the process of data analysis, it is crucial to differentiate between signals originating from gamma rays and cosmic rays. The traditional approach is to parameterize the image using Hillas parameters (length, width, orientation, etc.) [7]. As an empirical result, gamma rays produce images that are much longer and narrower than cosmic ray (mainly proton) lines. [8] However, when the energy is reduced, especially below 100 GeV, HADAR is poor in distinguishing them, resulting in the Hillas parameter method not being applicable.

To solve this problem, there are different methods, such as neural networks, random forests and so on. The multilayer perceptron (MLP) method [9] used in this study is a simple, fast and robust neural network algorithm. Based on the training data set, the MLP mimics biological neurons to build a mathematical model, and the optimal classification strategy is obtained through continuous iterative training. In this study, we used the MLP model provided by multivariate data analysis package (TMVA) [10] to improve the discrimination performance of gamma/proton in HADAR.

The structure of this paper is as follows: the second section briefly describes the HADAR experiment, the third section introduces the simulation parameters and MLP settings, the fourth section is the simulation results, and finally, the conclusion summarizes the entire paper.

2. HADAR Experiment

The HADAR is made up of four water lenses. Each water lens can detect the Cerenkov light with an energy range of 10 GeV to 10 TeV generated by cosmic rays or gamma-ray. The arrangement of the experiment is as shown on the left side of Figure 1. Specifically, four water lenses with a side length of 100 meters are arranged in a 2×2 square [11]. And the small white squares are plastic scintillator detectors located in the Yangbajing array. The scintillator can be detected in conjunction with the water lens. The design of a single water lens is shown in detail on the right side of Figure 1. At the top of the water lens is a crown-shaped acrylic lens with a diameter of 5 meters, below which sits a water tank with a radius of 4 meters and a height of 7 meters. The bottom of the tank is equipped with 18,961 photomultiplier tubes (PMTs) with a diameter of 5 cm each. The interior walls of the steel tank are coated with an absorbent material, while the exterior walls are coated with thermal insulation material. Inside the tank is pure water, which can collect Cherenkov light to the PMTs placed at the focal plane of the lens.

The reflection-based IACT has achieved many achievements in VHE gamma-rays observation. However, due to the configuration where the camera and incident light were on the same side in reflection-based IACT, the camera can obstruct some of the incoming light, necessitating a constraint on the camera size and consequently limiting the field of view of the reflection-based IACT. Due to the low field of view, the reflection-based IACT must take time to rotate to the specified position. Therefore, it is difficult to detect the prompt emission of gamma-ray bursts. Refractive IACT using a lens-based imaging system can boast a wider field of view. The HADAR experiment, with a field of view of 0.84 sr, possesses the potential to effectively detect transient radiation due to its expanded field of view.

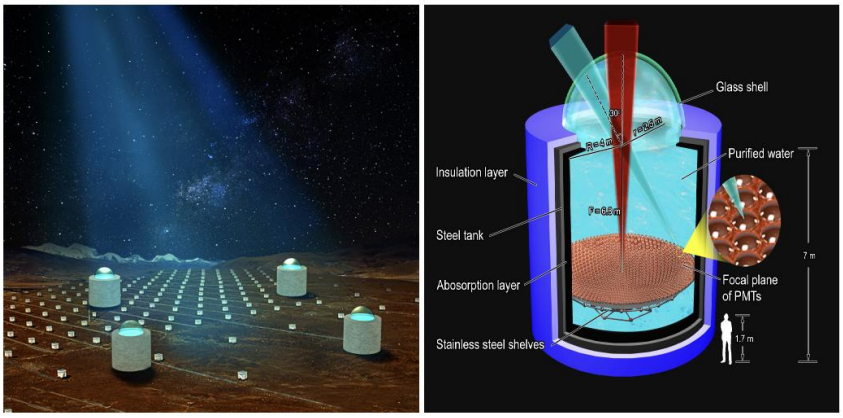

Left: distribution of the HADAR experimental setup. Right: design of a single water lens.[12]

Figure 1: Schematic diagram of the HADAR experiment

3. Simulation Method

3.1 HADAR Simulation Settings

The simulation of extensive air showers (EAS) for HADAR was completed using the Corsika software package (Version 74100), following the work of Xin GG [5], Qian XL [4], Chen QL [11], and others. The package adopted the atmospheric Cherenkov mode, where the high-energy part of the strong interaction model used QGSJETII 04 [13], low-energy part used Gheisha, and the electromagnetic component utilized EGS4 program. The simulation was set up at an altitude of 4300 meters, corresponding to an atmospheric depth of 606 g/cm^2, and at the geographic coordinates of Yangbajing (N30.0848, E90.5522). The primary cosmic ray particle energy range was set from 30 GeV to 100 GeV, with an incident zenith angle range of 0-30 ° and an azimuthal angle range of 0-360 °. All events were uniformly distributed within a circle with a radius of 400 meters centered on the HADAR array. Under these settings, the Corsika software package generated original data for the atmospheric Cherenkov light produced by EAS for subsequent simulation and analysis.

Regarding the trigger mode of the PMT, HADAR differs from other IACT experiments due to the wide field of view of the HADAR telescope, which introduces a significant amount of night sky background noise. Therefore, suppressing the numerous noise signals from the night sky background has become a bottleneck issue for the HADAR experiment. For high-energy events, the impact of night sky background noise is somewhat reduced because high-energy events generate a large number of Cherenkov photons. The signal from gamma photons is not likely to be drowned out by the night sky background noise. However, for low-energy events, they do not produce as many photons as high-energy events, and the faint Cherenkov photons can easily be overwhelmed by the noise. In order to improve the measurement of signals in the presence of night sky background noise, Xin GG et al. proposed a triggering algorithm suitable for HADAR. For more details on the triggering process, refer to [14], where the PMT trigger setting of this study aligns with theirs.

3.2 Hillas Parameters

Due to the large longitudinal spread and small transverse spread of air showers induced by gamma rays, the images in the camera appear elliptical, whereas cosmic ray-induced shower images are more dispersed, as shown in Figure 2. The shapes of these ellipses are typically described by the first and second moments of the image intensity distribution. Parameters used to characterize the ellipses and their orientation in the camera is known as Hillas parameters, which have become crucial parameters

in Cherenkov telescope event analysis.

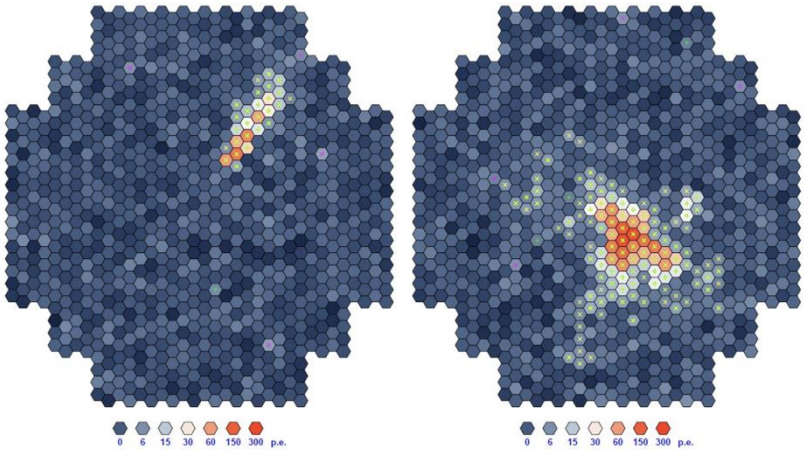

Left: a 1.0 TeV gamma-ray shower image, with a regular ellipse-like shape. Right: the image of a 2.6 TeV proton in the camera, with an irregular and more wide shape. Image couresy.[15]

Figure 2: Two example images of the light intensity distribution in the camera of the telescope

Figure 3 illustrates some parameters of the Hillas ellipse. Below we list some of the important parameters and provide a short description:

1) Center of gravity: The center of gravity of the image calculated from the distribution of photons on the camera, which is the center of the ellipse;

2) Length: length of the long axis of the Hillas ellipse;

3) Width: short axis length of Hillas ellipse;

4) α: the angle between the major axis of the ellipse and the line between the center of the ellipse and the center of the camera;

5) Size: the amount of charge accumulated on the camera by a single instance.

The Cherenkov light image after Hillas parameterization helps to identify the primary particles.

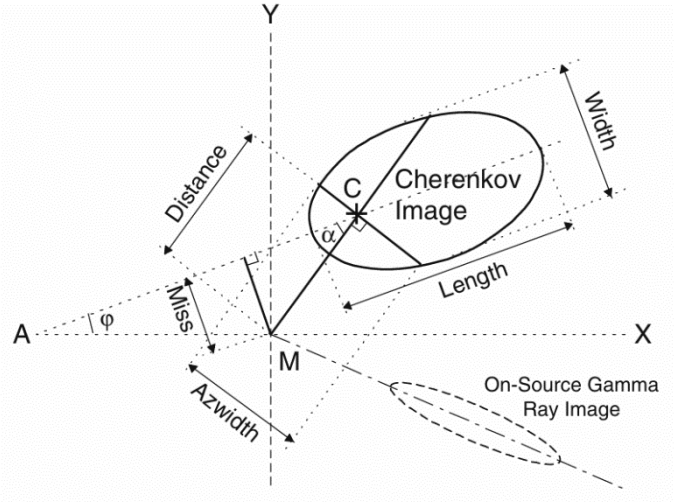

Figure 3[16]: Hillas definition of each parameter.

3.3 MLP Simulation Settings

The MLP model is, in fact, a simulation and simplification of biological neurons. The most typical MLP consists of three layers: the input layer, hidden layer, and output layer. MLP is usually applied to supervised learning problems, where it is trained on a set of input-output pairs and learns to model the correlations or dependencies between these inputs and outputs. The training involves adjusting the model's parameters or weights and biases to minimize errors as much as possible, as shown in Figure 4.

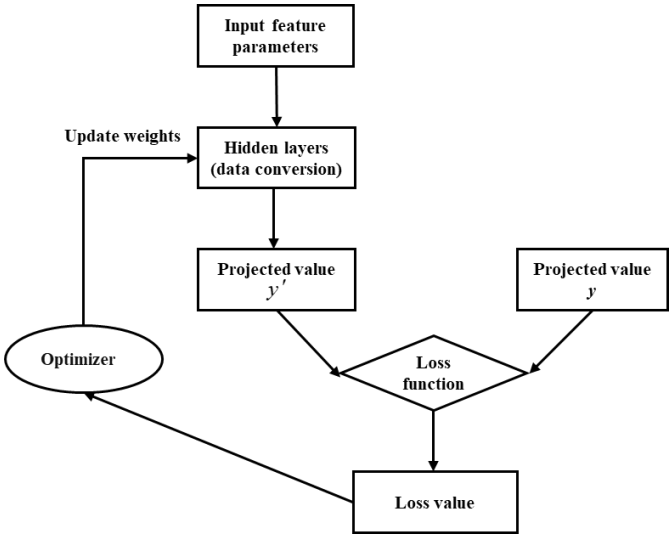

Figure 4: Schematic diagram of the MLP training process.

The MLP method used in this study was provided by the TMVA software package, which is part of the ROOT [17] data analysis framework (ROOT version 6.28). The following MLP settings were used in this study:

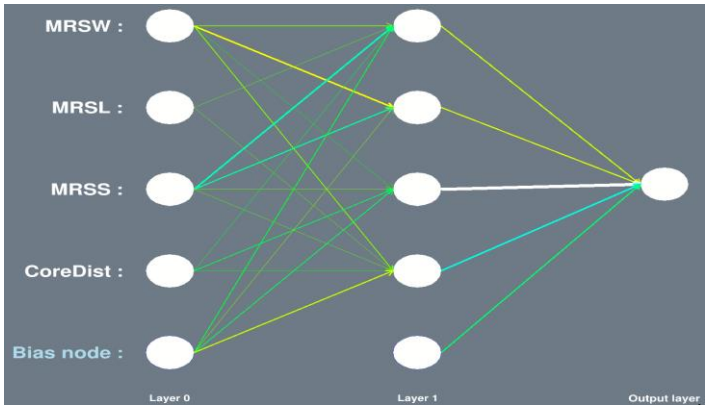

Figure 5: MLP model reference diagram, Layer 0 is the input parameter, Bias node is the bias node, Layer 1 is the hidden layer, Output layer is the output result(Outputs floating point numbers from 0 to 1, determines particle type based on cut conditions).

1) The input layer selected four feature parameters: MRSW (obtained by uniformly averaging and scaling the Hillas Width, referencing the simulation process in the HESS experiment [18]), MRSL (similar to MRSW, obtained by uniformly averaging and scaling the Hillas Length), MRSS (processed similarly to MRSW and MRSL using Hillas Size), and Core Dist (Core Distance, representing the distribution of core distances, inspired by the setup in reference [19]);

2) The activation function used was the Sigmoid function;

3) The hidden layer was set to 1 layer with 4 nodes, as illustrated in Figure 5;

4) To prevent overfitting and determine suitable numbers of test and training events, guidance from the TMVA manual's configuration instructions was consulted. From a dataset comprising 14530 gamma events and 13338 proton events, totaling 27868 events, 12000 events were randomly chosen for testing and training purposes.

4. Simulation Results

The relationship between the training loss function and the number of training epochs was illustrated in Figure 6. As the number of training epochs increased, the value of the loss function gradually converged. At 150th epochs, both the test and training sets were stable. Figure 7 shows the comparison of gamma and proton in four input parameters. For the convenience of comparison, the data were processed according to the data standardization principle of TMVA. It was observed that distinguishing between particle types based solely on a single parameter was challenging in the 30-100 GeV range. Among the parameters, Core Dist showed the best performance, followed by MRSL, while MRSW and MRSS exhibited poorer performance.

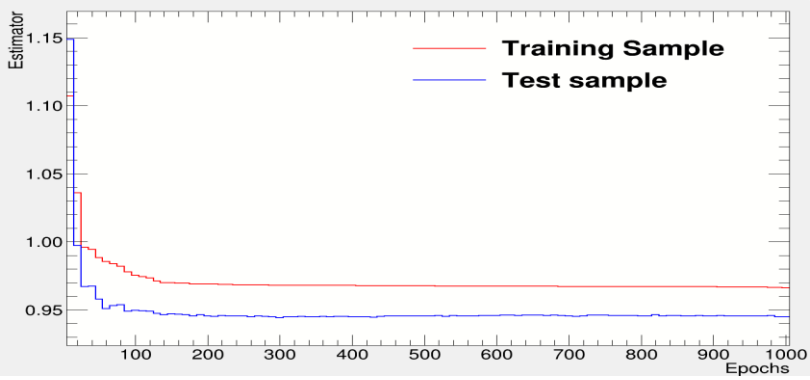

Figure 6: Loss function for MLP training and test data.

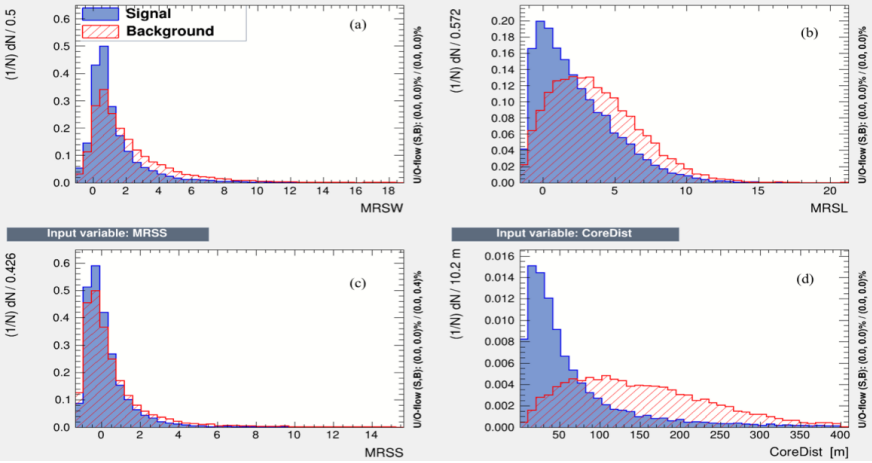

Figure 7: Comparison of the four input parameters for gamma and proton data, the data have been normalized according to TMVA's harmonization principles, with the blue shaded area being the signal (gamma) data and the red shaded area being the noise (proton) data.

Figure 8 shows the results after MLP training. After the MLP model was trained, the input of the four characteristic parameters yielded an output from the MLP. Based on this output, appropriate CUT conditions were chosen to determine the particle type. At that time, the separation performance was significantly better than any of the methods shown in Figure 7.

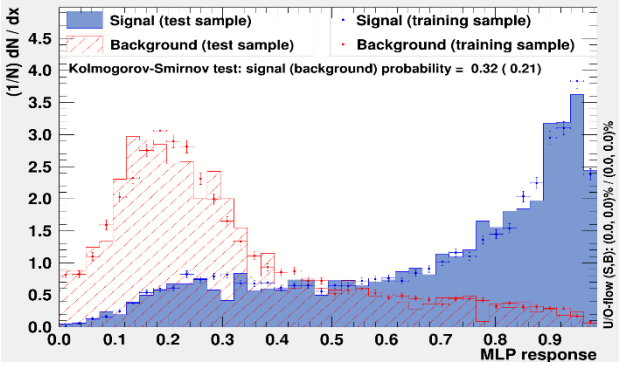

Figure 8: Results after MLP training, blue shaded areas are signal and red shaded areas are noise.

The overall goal of gamma/proton identification is to maximize the significance of the gamma source. Generally, a Quality Factor, also known as Q factor, is used to evaluate the quality of background inhibition. Q factor is calculated by Q=, is identifying the ratio of simulated gamma rays after selection to simulated gamma rays before selection, or the survival rate of gamma rays; is the ratio of the simulated proton after selection to the simulated proton before selection, representing the survival rate of the proton. Figure 9 shows the relationship between the Q factor and the CUT threshold for gamma/proton discrimination at 30-100 GeV. The maximum Q factor was 2.17, and the survival rate of gamma was 32.20% and the exclusion rate of proton was 97.80%.

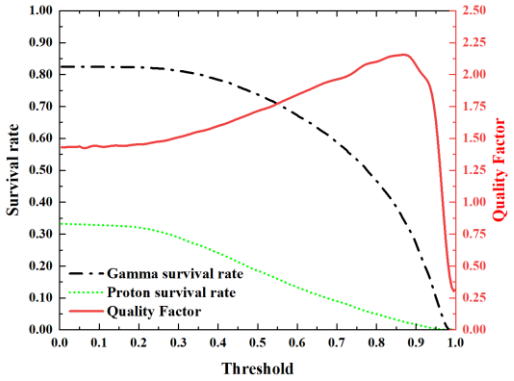

Figure 9: Relationship between Quality Factor and CUT threshold, where the black dotted line is the survival rate of gamma events, the green dotted line is the retention rate of protons, and the red solid line is the Quality Factor.

5. Conclusion

In this study, gamma/proton discrimination was achieved by utilizing an MLP model on the Monte Carlo simulated data for the HADAR experiment at 30-100 GeV. The approach integrated Hillas parameters, as well as the charge quantity of images and the distribution of core distance, enabling multivariate analysis. The findings indicated that, by choosing appropriate CUT thresholds, within the HADAR field of view, the maximum Q-factor reached 2.17, resulting in the exclusion of 97.80% of proton background. Consequently, this provided a valuable reference for enhancing gamma/proton discrimination in the HADAR experiment. It is hoped that the HADAR experiment will be established successfully in the future, and superior discrimination methods will be identified to enhance sensitivity towards observed sources.

Acknowledgement

Supported by the National Natural Science Foundation of China (1226030038).

References

[1] Sol, H., Zech, A., Boisson, C., Barres de Almeida, U., Biteau, J., Contreras, J.-L., Giebels, B., Hassan, T., Inoue, Y., Katarzyński, K., Krawczynski, H., Mirabal, N., Poutanen, J., Rieger, F., Totani, T., Benbow, W., Cerruti, M., Errando, M., Fallon, L., … White, R. (2013). Active Galactic Nuclei under the scrutiny of CTA. Astroparticle Physics, 43, 215–240. https://doi.org/10.1016/j.astropartphys.2012.12.005

[2] Gilmore, R. C., Bouvier, A., Connaughton, V., Goldstein, A., Otte, N., Primack, J. R., & Williams, D. A. (2012). IACT observations of gamma-ray bursts: prospects for the Cherenkov Telescope Array. Experimental Astronomy, 35(3), 413–457. https://doi.org/10.1007/s10686-012-9316-z

[3] López Coto, R. (2016). The Imaging Atmospheric Cherenkov Technique and the IACTs MAGIC and CTA. Springer Theses (pp. 15–64). Springer International Publishing. https://doi.org/10.1007/978-3-319-44751-3_2

[4] Qian, X., Sun, H., Chen, T., Feng, Y., Gao, Q., Gou, Q., Guo, Y., Hu, H., Kang, M., Li, H., Liu, C., Liu, M., Liu, W., Qiao, B., Wang, X., Wang, Z., Xin, G., Yao, Y., … Zhang, Y. (2022). Prospective study on observations of γ-ray sources in the Galaxy using the HADAR experiment. Frontiers of Physics, 17(6), 64602. https://doi.org/10.1007/s 11467-022-1206-x

[5] Xin, G. G., Yao, Y. H., Qian, X. L., Liu, C., Gao, Q., Luo, D. Z., Feng, Y. L., Gou, Q. B., Hu, H. B., Li, H. J., Liu, M. Y., Liu, W., Qiao, B. Q., Wang, Z., Zhang, Y., Cai, H., Chen, T. L., & Guo, Y. Q. (2021). Prospects for the Detection of the Prompt Very-high-energy Emission from γ-ray Bursts with the High Altitude Detection of Astronomical Radiation Experiment. The Astrophysical Journal, 923(1), 112. https://doi.org/10.3847/1538-4357/ac2df7

[6] Cronin, J. W. (1999). Cosmic Rays: The Most Energetic Particles in the Universe (pp. 278–290). Springer New York. https://doi.org/10.1007/978-1-4612-1512-7_17

[7] Kwok, P. W., Cawley, M. F., Fegan, D. J., Gibbs, K. G., Hillas, A. M., Lamb, R. C., Lewis, D. A., Macomb, D., Porter, N. A., Reynolds, P. T., Vacanti, G., & Weekes, T. C. (1989). Observation of TeV Gamma-rays from the Crab Nebula (pp. 245–252). Springer Netherlands. https://doi.org/10.1007/978-94-009-0921-2_17

[8] Postnikov, E. B., Kryukov, A. P., Polyakov, S. P., Shipilov, D. A., & Zhurov, D. P. (2019). Gamma/Hadron Separation in Imaging Air Cherenkov Telescopes Using Deep Learning Libraries TensorFlow and PyTorch. Journal of Physics: Conference Series, 1181, 012048. https://doi.org/10.1088/1742-6596/1181/1/012048

[9] Taud, H., & Mas, J. F. (2018). Multilayer Perceptron (MLP) (pp. 451–455). Springer International Publishing. https://doi.org/10.1007/978-3-319-60801-3_27

[10] Voss, H., Höcker, A., Stelzer, J., & Tegenfeldt, F. (2009, July). TMVA, the Toolkit for Multivariate Data Analysis with ROOT. Proceedings of XI International Workshop on Advanced Computing and Analysis Techniques in Physics Research — PoS(ACAT). https://doi.org/10.22323/1.050.0040

[11] Chen, Q. L., Hu, P. J., Su, J. J., Kang, M. M., Guo, Y. Q., Chen, T. L., Luo, D. Z., Fan Y. F., Feng, Y. L., Gao, Q., Gou, Q. B., Hu, H. B., Li, H. J., Liu, C., Liu, M. Y., Liu, W., Qian, X. L., Qiao, B. Q., Sun, H. Y., … Zhao, B. (2023). Prospects for the detection rate of very-high-energy γ-ray emissions from short γ-ray bursts with the HADAR experiment. Chinese Physics C, 47(9), 095001. https://doi.org/10.1088/1674-1137/ace3ac*

[12] Heck, D., Knapp, J., Capdevielle, J. N., Schatz, G., & Thouw, T. (1998). CORSIKA: A Monte Carlo code to simulate extensive air showers [Techreport]. https://doi.org/10.5445/IR/270043064

[13] Ostapchenko, S. (2006). QGSJET-II: towards reliable description of very high energy hadronic interactions. Nuclear Physics B - Proceedings Supplements, 151(1), 143–146. https://doi.org/https://doi.org/ 10.1016/j. nuclphysbps. 2005.07.026

[14] Xin, G. G., Cai, H., Guo, Y. Q., Chen, T. L., Liu, C., & Qian, X. L. (2022). A novel trigger algorithm for wide-field-of-view imaging atmospheric Cherenkov technique experiments. Nuclear Science and Techniques, 33(3), 25. https://doi.org/10.1007/s41365-022-01003-3

[15] Völk, H. J., & Bernlöhr, K. (2009). Imaging very high energy gamma-ray telescopes. Experimental Astronomy, 25(1), 173–191. https://doi.org/10.1007/s10686-009-9151-z

[16] Sciascio, G. D. (2019). Ground-based Gamma-Ray Astronomy: an Introduction. Journal of Physics: Conference Series, 1263(1), 012003. https://doi.org/10.1088/1742-6596/1263/1/012003

[17] Antcheva, I., Ballintijn, M., Bellenot, B., Biskup, M., Brun, R., Buncic, N., Canal, Ph., Casadei, D., Couet, O., Fine, V., Franco, L., Ganis, G., Gheata, A., Maline, D. G., Goto, M., Iwaszkiewicz, J., Kreshuk, A., Segura, D. M., Maunder, R., … Tadel, M. (2011). ROOT — A C++ framework for petabyte data storage, statistical analysis and visualization. Computer Physics Communications, 182(6), 1384–1385. https://doi.org/10.1016/j.cpc.2011.02.008

[18] Benbow, W., & Collaboration, H. E. S. S. (2005). The Status and Performance of H.E.S.S. AIP Conference Proceedings, 745(1), 611–616. https://doi.org/10.1063/1.1878471

[19] Krause, M., Pueschel, E., & Maier, G. (2017). Improved γ/hadron separation for the detection of faint γ-ray sources using boosted decision trees. Astroparticle Physics, 89, 1–9. https://doi.org/10.1016/j.astropartphys. 2017. 01. 004